

Origins of suppressed self-diffusion of nanoscale constituents of a complex liquid

Christian P. N. Tanner,¹ Vivian R. K. Wall,¹ Mumtaz Gababa,¹ Joshua Portner,² Ahhyun Jeong,² Matthew J. Hurley,^{3,*} Nicholas Leonard,³ Jonathan G. Raybin,¹ James K. Utterback,^{1,†} Ahyoung Kim,^{1,‡} Andrei Fluerasu,⁴ Yanwen Sun,⁵ Johannes Möller,⁶ Alexey Zozulya,⁶ Wonhyuk Jo,⁶ Felix Brausse,⁶ James Wrigley,⁶ Ulrike Boesenberg,⁶ Wei Lu,⁶ Roman Shayduk,⁶ Mohamed Youssef,⁶ Anders Madsen,⁶ David T. Limmer,^{1,7,8} Dmitri V. Talapin,^{2,9} Samuel W. Teitelbaum,³ and Naomi S. Ginsberg^{1,10,11,12,8,13,§}

¹*Department of Chemistry, University of California, Berkeley, CA 94720, USA*

²*Department of Chemistry, James Franck Institute,*

and Pritzker School of Molecular Engineering, University of Chicago, Chicago, IL 60637, USA

³*Department of Physics, Arizona State University, Tempe, AZ 85287, USA*

⁴*Brookhaven National Laboratory, NSLS-II, Upton, NY 11973, USA*

⁵*Linac Coherent Light Source, SLAC National Accelerator Laboratory, Menlo Park, CA 94025, USA*

⁶*European X-ray Free-Electron Laser Facility, Holzkoppel 4, 22869 Schenefeld, Germany*

⁷*Chemical Sciences and Materials Sciences Divisions,*

Lawrence Berkeley National Laboratory, Berkeley, CA 94720, USA

⁸*Kavli Energy NanoSciences Institute, University of California, Berkeley, CA 94720, USA*

⁹*Center for Nanoscale Materials, Argonne National Laboratory, Argonne, IL 60517, USA*

¹⁰*Department of Physics, University of California, Berkeley, CA 94720, USA*

¹¹*Molecular Biophysics and Integrated Bioimaging Division,*

Lawrence Berkeley National Laboratory, Berkeley, CA 94720, USA

¹²*Materials Sciences and Chemical Sciences Division,*

Lawrence Berkeley National Laboratory, Berkeley, CA 94720, USA

¹³*STROBE, NSF Science & Technology Center, Berkeley, CA 94720, USA*

The ability to understand and ultimately control the transformations and properties of various nanoscale systems, from proteins to synthetic nanomaterial assemblies, hinges on the ability to uncover their dynamics on their characteristic length and time scales. Here, we use MHz X-ray photon correlation spectroscopy (XPCS) to directly elucidate the characteristic microsecond-dynamics of density fluctuations of semiconductor nanocrystals (NCs), not only in a colloidal dispersion but also in a liquid phase consisting of densely packed, yet mobile, NCs with no long-range order. We find the wavevector-dependent fluctuation rates in the liquid phase are suppressed relative to those in the colloidal phase and relative to observations of densely packed repulsive particles. We show that the suppressed rates are due to a substantial decrease in the self-diffusion of NCs in the liquid phase, which we attribute to explicit attractive interactions. Using coarse-grained simulations, we find that the extracted shape and strength of the interparticle potential explains the stability of the liquid phase, in contrast to the gelation observed via XPCS in many other charged colloidal systems. This work opens the door to elucidating fast, condensed phase dynamics in complex fluids and other nanoscale soft matter, such as densely packed proteins and non-equilibrium self-assembly processes, in addition to designing microscopic strategies to avert gelation.

Equilibrium fluctuations of a system's microscopic parameters encode its nonequilibrium response to perturbations [1]. For example, a system's equilibrium density field fluctuations or individual particle velocities encode the nature of their transport, and analogous relations exist for charge, volume, and heat flow[2]. Knowing and manipulating how microscopic equilibrium fluctuations control these emergent nonequilibrium properties thus enables direct control over dynamical system properties. One important example of this connection is determining how the microscopic hydrodynamic, i.e., solvent-mediated, interactions of particles in a colloidal suspension change as a function of the interactions between the particles and their concentration [3–5]. While much work has gone into understanding the hydrodynamic interactions of model systems, such as ensembles of repulsive spheres, [6–10] interactions between particles in complex fluids (e.g., nanocrystal assemblies, pro-

teins, polymers) are often more difficult to predict due to the more elusive nature of their many-body interactions. Clarifying and ultimately controlling the interactions between particles in these complex fluids requires directly elucidating their dynamics on their characteristic time- and length scales.

Measuring the dynamics of many complex fluid systems is challenging due to their small length scales (nm) and fast time scales (μs). Typically, the dynamics associated with translational, vibrational, or rotational motion of micron-scale particles are measured in the time domain with optical scattering or optical microscopy techniques [12–17]. For atomic systems, these dynamics are measured in the frequency domain using inelastic X-ray or neutron scattering techniques that are limited to ns or shorter time scales [18]. MHz X-ray photon correlation spectroscopy (XPCS) at the European X-ray free electron laser (XFEL) offers the ability to measure dynam-

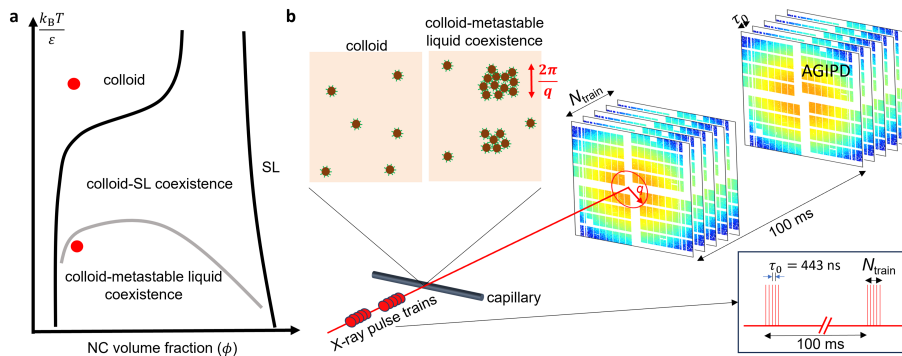


Figure 1. Overview of MHz XPCS experiment. **a.** Phase diagram of PbS NCs as a function of NC volume fraction (ϕ) and quench depth ($k_B T/\epsilon$, where k_B is Boltzmann’s constant, T is temperature and ϵ is depth of interparticle interactions) [11]. The solid curves indicate the colloid-SL (black) and colloid-metastable liquid (grey) phase coexistence boundaries (SL indicates a solid phase of NCs). Red circles represent states that were measured in XPCS. **b.** Ultrafast X-ray pulses are delivered to the sample consisting of a solution of NCs in a glass capillary. As the NCs fluctuate in solution, they scatter the X-rays onto the AGIPD detector that is synchronized to the incident X-ray pulses. The X-ray pulses are structured in pulse trains, consisting of N_{train} pulses at a $1/\tau_0=2.2$ MHz repetition rate. In this schematic, $N_{\text{train}} = 5$, but in the experiments, $N_{\text{train}} = 50$. The first pulse in each pulse train is separated by 100 ms from the first pulse in the preceding pulse train. Correlation analysis is performed within each pulse train and then averaged over the ~ 100 s of pulse trains within a measurement.

ics on microsecond time scales, [19, 20] filling an important gap between these previously available techniques. XPCS is a time-domain coherent X-ray scattering technique that measures density fluctuations in reciprocal space [7, 18, 21–25]. In order to generate high enough signal-to-noise ratio in the scattered signal, high intensity X-rays are required, which in turn can damage a sample and influence its dynamics [10, 20, 26]. As a result, special care is required to understand and minimize X-ray induced effects when using XPCS [20, 26, 27].

Despite the fast time- and short length scales of nanoscale systems, we directly elucidate the dynamics associated with density fluctuations of few-nanometer-diameter charged semiconductor nanocrystals (NCs) as a function of their volume fraction and interaction strength using MHz XPCS. By changing the ionic strength of the dispersing solution of this complex fluid, we tune the electrostatic repulsion between the charged NCs, thereby controlling the strength of their interactions. As a result, we are able to generate both stable colloidal and liquid phases [11, 28]. The liquid phase consists of densely packed, mobile NCs with no long-range order. By developing analysis methods, we carefully disentangle the intrinsic dynamics of the NCs in the colloidal and liquid phases from the X-ray induced effects on the system. In combination with theoretical methods, we extract the self-diffusion coefficient [1] of the NCs as a function of their volume fraction and interaction strength and find that the self-diffusion coefficient of NCs in the liquid phase is suppressed relative to that of hard spheres [8] and charged spheres [8] at the same volume fraction. We show that this suppression can be explained through a combination of hydrodynamic and explicit attractive interactions between NCs, and we extract the strength of their interactions via direct comparison with simulations. The $\sim 2 k_B T$ attractive interaction strength of the NCs

explains the stability of this liquid phase. By comparing to other nanoscale and microscale complex fluids, we also infer the shape of the nanoscale interparticle interaction potential, which explains why these NCs avoid kinetic arrest or gelation following quenches from the colloidal phase, as compared to microscale systems. The combination of experiment, analysis, theory, and simulation enables us to determine the system’s transport properties and interactions, and similar approaches should now be able to directly elucidate similar properties of other complex fluids, such as polymer systems [29, 30] and proteins under physiological, cellular conditions [26, 31].

To determine the interactions between NCs in complex fluid phases, we study 5.8 ± 0.3 nm diameter PbS NCs coated with $\text{Sn}_2\text{S}_6^{4-}$ ligands dispersed in a mixture of N-methylformamide (NMF) and N,N-dimethylformamide (DMF) [28, 32]. In addition to studying the NCs in the colloidal phase (**Figure 1a**, upper red circle, **1b** inset), we quench the system via addition of a K_3AsS_4 salt solution that screens the electrostatic repulsion of the highly charged NCs that initially stabilizes them in the colloidal phase. As a result, the quenched state consists of colloidal NCs in coexistence with NCs in a metastable liquid phase (**Figure 1a**, lower red circle, **1b** inset) [11]. To measure the structure and dynamics of NCs in the colloidal and liquid phases, we use MHz XPCS at the Materials Imaging and Dynamics (MID) instrument at the European XFEL (**Figures 1, S1**) [33–35]. The NC solutions scatter X-rays generated from pulse trains consisting of $N_{\text{train}} = 50$ ultrafast (~ 50 fs duration), spatially coherent X-ray pulses at a 2.2 MHz repetition rate onto the detector [36] located 7 m from the sample. By azimuthally integrating detector images like in **Figure 2a**, we obtain one-dimensional SAXS patterns, $I(q)$, which describe the scattered X-rays’ intensity as a function of momentum transfer, q (**Figure 2b**). By fitting the

background-subtracted SAXS patterns to models of colloidal and liquid phases (**Figure S2, Methods**), we extract the NC size distribution and liquid phase NC volume fraction, which is 0.3 for the example in **Figure 2b**.

To obtain the characteristic dynamics associated with density fluctuations of the NCs, we calculate two-time correlation functions, $C(q, t_1, t_2)$, according to

$$C(q, t_1, t_2) = \frac{\langle \delta I(\mathbf{q}, t_1) \delta I(\mathbf{q}, t_2) \rangle_{\mathbf{q}}}{\langle I(\mathbf{q}, t_1) \rangle_{\mathbf{q}} \langle I(\mathbf{q}, t_2) \rangle_{\mathbf{q}}},$$

where $\delta I(\mathbf{q}, t_1) = I(\mathbf{q}, t_1) - \langle I(\mathbf{q}, t_1) \rangle_{\mathbf{q}}$ and $\langle \dots \rangle_{\mathbf{q}}$ denotes an average over \mathbf{q} -values that share a given magnitude of q . The two-time correlation functions $C(q, t_1, t_2)$ were calculated over the 50 pulses within each pulse train and then averaged across all pulse trains for each experiment (see **Methods**). Examples of $C(q, t_1, t_2)$ for the NCs in the colloidal and liquid phases are shown in **Figure 3a**. [37] The distance along the diagonal of the plots in **Figure 3a** indicates the age, $t = (t_1 + t_2)/2$, of the sample within the pulse train, i.e., how many pulses the sample has sustained. Following the value of $C(q, t_1, t_2)$ as it extends perpendicular to the diagonal provides the decay of the correlation function at a fixed age. The antidiagonal decay of $C(q, t_1, t_2)$ also depends on t , indicating that the sample dynamics change as more X-ray pulses within a pulse train interact with the sample. To quantify these dynamics, we calculate autocorrelation functions, $g^{(2)}$, from $C(q, t_1, t_2)$ at a fixed average sample age, \bar{t} (see **Methods**). For each phase, autocorrelation functions for $q = 0.016$ (mauve) to 0.030 (purple) \AA^{-1} using averages over the first 10 X-ray pulses ($0 \leq t \leq 8.86 \mu\text{s}$) in each pulse train are shown as points plotted in **Figure 3b**. The autocorrelation functions of the colloidal and liquid phases decay faster at higher q values and decay more slowly in the liquid phase than the colloidal phase.

To extract the rate at which density fluctuations decorrelate, we fit an exponential model [38], $g^{(2)}(q, \tau, \bar{t}) =$

$1 + \beta(q) \exp[-2\Gamma(q, \bar{t})\tau]$ (solid curves in **Figure 3b**), to the autocorrelation functions and obtain $\Gamma(q, \bar{t})$ (see **Methods, Figure S3**). The autocorrelation functions vary as a function of \bar{t} (**Figure S4a**). To obtain the decorrelation rate associated with the unperturbed NC dynamics, we extrapolate $\Gamma(q, \bar{t})$ to $\bar{t} \rightarrow 0$ (**Figure S4b**). The experimentally-determined rates, $\Gamma(q, \bar{t} = 4.43 \mu\text{s})$ (open circles) and $\Gamma(q, \bar{t} \rightarrow 0)$ (closed circles), are shown in **Figure 3c** in relation to the static structure factors, $S^c(q)$ and $S^\ell(q)$, which describe the modulation in the measured scattered X-ray intensity due to the spatial arrangement of NCs in the colloidal and liquid phases, respectively (see **Methods, Figure S5**). Here, $S^c(q) \sim 1$ (**Figure 3c**, black points), indicating the NCs are far apart and do not interact in the colloidal phase (see Ref. [32] for more details on $S^c(q)$ of these NCs). The liquid phase structure factor, $S^\ell(q)$, has a distinct peak at $q \sim 0.1 \text{\AA}^{-1}$ corresponding to a $\sim 6.3 \text{ nm}$ distance between neighboring NCs (**Figure 3c**, blue points). The ~ 1.7 height of this peak satisfies the Hansen-Verlet criterion for a liquid [39]. The decorrelation rates $\Gamma(q, \bar{t} \rightarrow 0)$ and $\Gamma(q, \bar{t} = 4.43 \mu\text{s})$ are ~ 1 order of magnitude larger for the colloidal phase than the liquid.

To quantify these trends, we fit $\langle D_{\text{eff}}^i \rangle q^2$ to $\Gamma(q, \bar{t} \rightarrow 0)$ (solid red curves in **Figure 3c**) for $i \in \{c, \ell\}$, where $\langle D_{\text{eff}}^i \rangle$ is an effective diffusivity averaged over the fit q -range. We find $\langle D_{\text{eff}}^c \rangle = 57 \mu\text{m}^2/\text{s}$ and $\langle D_{\text{eff}}^\ell \rangle = 5 \mu\text{m}^2/\text{s}$. To relate these effective diffusivities to real diffusion coefficients, we first relate $D_{\text{eff}}^i(q)$ to the hydrodynamic functions, $H^i(q)$, via $D_{\text{eff}}^i(q) = D_0 H^i(q) / S^i(q)$ [4, 40]. Here, $D_{\text{eff}}^i(q) = \Gamma(q, \bar{t} \rightarrow 0) / q^2$, D_0 is the self-diffusion coefficient of dilute NCs, and $H^i(q)$ encodes the direct, as well as the hydrodynamic, i.e., solvent-mediated, interactions between NCs. It is a many-body function that depends on all of the NCs in the system (see **Methods**). To extract $H^i(q)$ from the experimental data, we use the measured colloidal and liquid structure factors $S^i(q)$, $D_{\text{eff}}^i(q)$, and D_0 obtained from dynamic light scattering (DLS) measurements of the NCs at a volume fraction of 0.0002 (**Figure S6**). There is minimal to no evidence of interactions between the NCs in the colloidal phase, as $H^c(q) \sim 1$ (**Figure 4a**, black points). Yet, we find the values obtained for $H^\ell(q)$ for the NCs in the liquid phase (**Figure 4a** blue points) are all below 1.

Despite the influence of the extremely bright X-ray pulses on the sample, we are able to disentangle the X-ray induced effects from the intrinsic NC dynamics. The decorrelation rates that we extract (**Figure 3c**) are not due to concentration fluctuations of NCs in the X-ray probe volume since these are q -independent contributions that occur on longer time scales (**Figure S7**) that are normalized out in calculating $C(q, t_1, t_2)$. In addition, while the decorrelation rates increase with \bar{t} , we follow the process developed via a first principles calculation by Lehmkuhler et al. [20] (see **Methods, Figures**

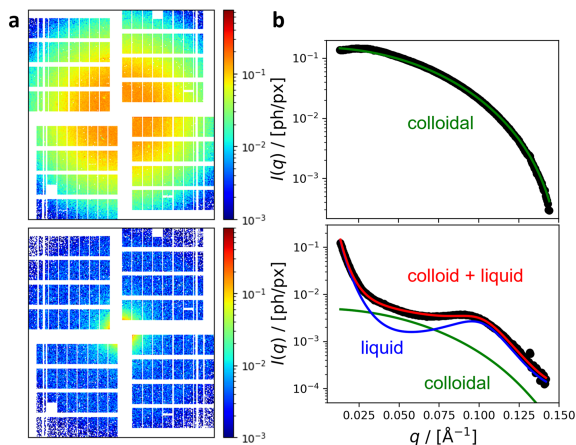


Figure 2. Static scattering of NCs. **a**. Detector images of scattering in the colloidal (top) and quenched (bottom) phases averaged over several pulse trains. **b**. Background-subtracted one-dimensional SAXS patterns, $I(q)$, in units of photons per pixel, of NCs in the colloidal (top) and quenched (bottom) phases (black points). Solid curves indicate fits to the SAXS patterns and components (as labeled).

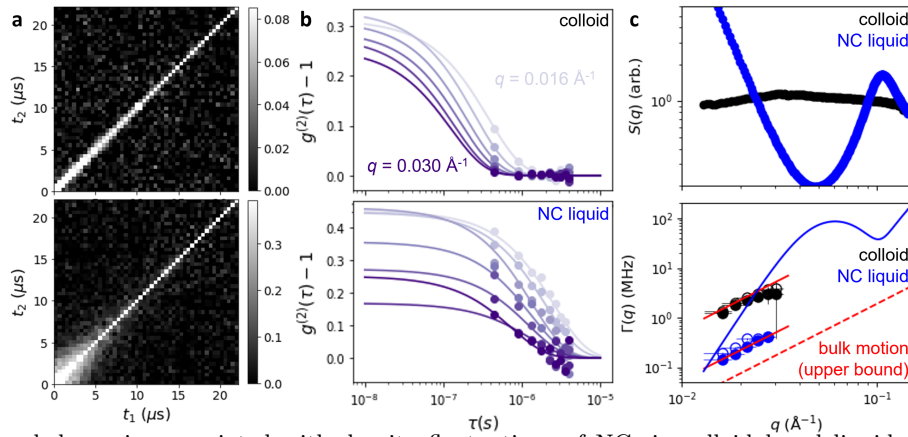


Figure 3. Microsecond dynamics associated with density fluctuations of NCs in colloidal and liquid phases. **a.** Two-time correlation functions, $C(q, t_1, t_2)$, for NCs in the colloidal (top) and liquid (bottom) phases at $q = 0.016 \text{ \AA}^{-1}$. **b.** Autocorrelation functions, $g^{(2)}(q, \tau, \bar{t} = 4.43 \text{ \mu s})$ as an increasing function of q (light to dark purple) for NCs in the colloidal (top) and liquid (bottom) phases (purple points). Solid curves are exponential fits to the data points. **c.** Colloidal and liquid phase structure factors, $S^c(q)$ and $S^l(q)$ (top), and decorrelation rates, $\Gamma(q)$ (bottom), for NCs in the colloidal (black) and liquid (blue) phases. The green curve in the upper panel is a fit of our liquid-phase scattering model to $S^l(q)$. Open circles in the lower panel indicate $\Gamma(q, \bar{t} = 4.43 \text{ \mu s})$ and solid circles indicate $\Gamma(q, \bar{t} \rightarrow 0)$. Solid red curves are fits to $\Gamma(q) = \langle D_{\text{eff}}^i \rangle q^2$. Dashed red curve represents the decorrelation rate expected for bulk motion of $\sim 90 \text{ nm}$ liquid droplets. Solid blue curve is the expected rate for NCs in the liquid phase in the absence of attractive and hydrodynamic interactions ($\Gamma(q) = D_0 q^2 / S^l(q)$).

S8, S9) to approximate the decorrelation rates in the absence of this temperature increase via extrapolation. Furthermore, using the $\langle D_{\text{eff}}^c \rangle = 57 \text{ \mu m}^2/\text{s}$ obtained for the NCs in the colloidal phase, the hydrodynamic diameter predicted through the Einstein-Smoluchowski relation is 6.2 nm . This value agrees with DLS (**Figure S6**) and the lattice constant of solid ordered arrays of the NCs[11]. Finally, we estimate the size of individual liquid droplets to be ~ 30 times larger than the individual NCs (**Figure S10**). Thus, the measured liquid-phase decorrelation rates are much too fast to be due to bulk motion of liquid droplets (**Figure 3c**, dashed red curve).

Having determined the effective diffusion coefficient and hydrodynamic functions of NCs in the colloidal and liquid phases, we consider the underlying interactions consistent with the observed dynamics. The ratio of the self-diffusion coefficient, D_s^i , to D_0 is given by $H^i(q \rightarrow \infty)$. For NCs in the colloidal phase, we found $H^c(q) \sim 1$ at all q , indicating that $D_s^c/D_0 = 1$ (**Figure 4b** red x's). These values of D_s^c/D_0 fall on the expected trend for charged spheres (**Figure 4b** purple curve) [8]. Since our experimental data and analysis do not sufficiently approach $q \rightarrow \infty$ to extract D_s^l/D_0 , we instead consider two complementary approaches. The first is the $\delta\gamma$ -method of Beenakur and Mazur [43, 44] (solid curves in **Figure 4a**, see **Methods**). Within our measured q -range we find the shape of $H^l(q)$ is reasonably well-described by the $\delta\gamma$ -method, but that a value of $D_s^l/D_0 = 0.23$ must be included to fit the data (see **Methods**). For the second approach, we performed Brownian dynamics simulations of NCs in a liquid phase interacting with various well depths ϵ and extracted $H^l(q)$ (**Figure 4a** red points, **Figure S11**, see **Methods**). We find the extracted $H^l(q)$ from our simulations using $\epsilon \sim 2 k_B T$

agrees with the experimentally-determined $H^l(q)$, and we extract $D_s^l/D_0 = 0.18$ for the simulated NCs (**Figure S12**). These two values of D_s^l/D_0 (**Figure 4b** red points) both fall below the experimentally verified values for hard spheres (**Figure 4b**, black curve) and charged spheres (**Figure 4b**, purple curve) [8]. Given that the NCs are only an order of magnitude larger than the surrounding ion and solvent molecules, the NC solvation shell fluctuations may well play a role in suppressing the NC self-diffusion, especially as compared to larger, e.g., micron-sized, particles. Nevertheless, given the agreement between experiment and the Brownian dynamics simulations, we postulate that explicit attractive interactions between the NCs are predominantly responsible for the suppressed value of D_s^l/D_0 .

Importantly, the simulated $\epsilon = 2 k_B T$ NC-NC interaction strength consistent with our experimental data analysis is also consistent with values predicted from previous studies on these NCs[11] and from simulations [45] of coarse-grained NCs and explains the stability of this liquid phase: in contrast to other NC systems following a quench out of the colloidal state, [46, 47] the relatively shallow interaction strengths of the present NCs prevent their arrest in a glassy or gel-like state. This stability is crucial for the self-assembly of these NCs into ordered structures for optoelectronic applications.[11, 28, 48–53] In addition, the values of D_s^i/D_0 for the NCs in the colloidal and liquid phases could be used in rate expressions [11, 54–56] to predict and ultimately control self-assembly kinetics, which is crucial to create defect-free structures. Further corroborating the experimental findings with simulations that also incorporate hydrodynamics [8, 57–59] and extending the q range over which to compare our system with models for $H^i(q)$ will assist in

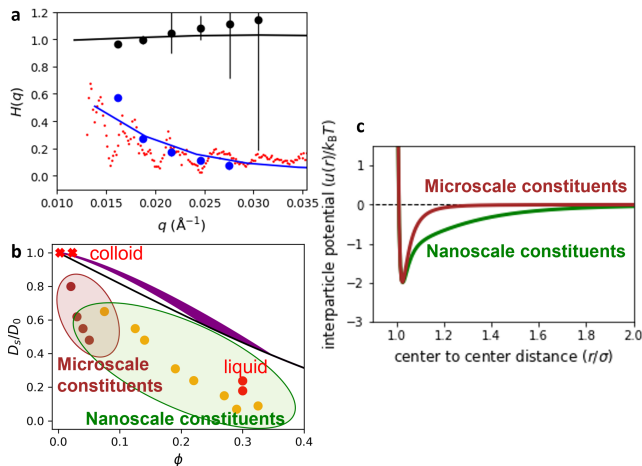


Figure 4. Microscopic fluctuations of NCs as a function of their density and interaction strength. **a.** Hydrodynamic functions, $H^i(q)$, for NCs in the colloidal (black points) and liquid (blue points) phases. Solid curves are predictions of $H^i(q)$ based on the $\delta\gamma$ -method with a modified self-diffusion coefficient for NCs in the liquid phase (see **Methods**). Red points are results of Brownian dynamics simulations of NCs interacting with a Lennard-Jones potential with a well depth $\epsilon = 2 k_B T$ (oscillations are due to finite size of simulated liquid droplet). **b.** Self-diffusion coefficient of NCs in colloidal phase at two different volume fractions (red x's) and NCs in liquid phase (red circles) extracted via $\delta\gamma$ -method ($D_s^l/D_0=0.23$) and via comparison to simulation ($D_s^l/D_0=0.18$). Solid curves are relationships between D_s^c/D_0 and NC volume fraction (ϕ) for charged spheres [8] (purple) and hard spheres [8] (black). Gold and brown points are results from protein experiments [41] and micron-scale colloid-polymer mixtures [42], respectively **c.** Schematic interparticle potentials of nanoscale and microscale particles as a function of particle center-to-center distance particles, normalized to particle size σ .

refining our intuition about the microscopic source of the suppressed diffusivities.

Returning to the degree of suppressed self-diffusion, in addition to our finding for the NC liquid phase, the D_s/D_0 trends for colloid-polymer mixtures with attractive depletion interactions [42] (**Figure 4b** brown data points) and proteins [41] (**Figure 4b** gold points) also fall below the expected values for hard spheres and charged spheres. The D_s^l/D_0 for liquid-phase NCs in this work is similar to that of proteins at the same volume fraction (ϕ). The D_s/D_0 values for the colloids interacting with polymer depletants are larger and are constrained to much lower ϕ due to the onset of gelation before metastable liquid formation can occur. This finding suggests a difference between the interactions of measured nanoscale and microscale constituents of the complex liquids, even though systems at both scales are typically thought to have the same interparticle interactions relative to their constituents' size. Simulations that phenomenologically introduced a long-range attractive tail to short-range attractive potentials previously showed that this tail could be used to avert the onset of gelation at low ϕ [60]. Based on these and explicit calculations of interparticle interactions using Derjaguin-Landau-Verwey-

Overbeek (DLVO) theory [61] and the Asakura-Oosawa model [62–64] (**Figure S13**), we propose that nanoscale interparticle interactions, $u(r)$, likely have long-range attractive tails that are absent in the interparticle interactions of microscale particles measured to-date (**Figure 4c**). This finding provides a strategy to either avoid or enhance gelation during self-assembly of nanoscale and microscale systems, provided the shape and depth of constituents' interparticle interactions can be sufficiently tuned. By validating MHz XPCS on constituent characteristic length- and time scales, this work thus paves the way to more generally inferring important interactions in a wide range of complex fluids. These could be treated directly or by using systems like the NCs in this work as models for more damage-prone complex fluids, such as biomolecular condensates, whose high-resolution fluctuations are elusive to diffraction-limited optical microscopy.

ACKNOWLEDGMENTS

We thank A. Omar and E. Weiner for discussions. This work was supported by the Office of Basic Energy Sciences (BES), US Department of Energy (DOE) (award DE-SC0019375). We acknowledge the European XFEL in Schenefeld, Germany, for provision of XFEL beamtime at Scientific Instrument MID (Materials Imaging and Dynamics) under proposal 3049. C.P.N.T. and V.R.K.W. were supported by the NSF Graduate Research Fellowship. J.K.U. was supported by an Arnold O. Beckman Postdoctoral Fellowship in Chemical Sciences. D.T.L. was supported by an Alfred P. Sloan Research Fellowship. N.S.G. was supported by a David and Lucile Packard Foundation Fellowship for Science and Engineering and Camille and a Henry Dreyfus Teacher-Scholar Award.

* Present Address: Department of Physics, Stanford University, Stanford, CA 94305, USA

† Present Address: Sorbonne Université, CNRS, Institut des NanoSciences de Paris, INSP, 75005 Paris, France

‡ Present Address: California Institute of Technology, Pasadena, CA 91125, USA

§ nsginsberg@berkeley.edu

- [1] P. M. Chaikin and T. C. Lubensky, *Principles of Condensed Matter Physics* (Cambridge University Press, Cambridge, 1995).
- [2] D. T. Limmer, *Statistical mechanics and stochastic thermodynamics: A textbook on modern approaches in and out of equilibrium* (Oxford University Press, 2024).
- [3] R. B. Jones and P. N. Pusey, Annual Review of Physical Chemistry **42**, 137 (1991), publisher: Annual Reviews.
- [4] G. Nägele, Physics Reports **272**, 215 (1996).
- [5] J. F. Brady, The Journal of Chemical Physics **99**, 567 (1993).
- [6] A. J. C. Ladd, The Journal of Chemical Physics **93**, 3484 (1990).
- [7] D. Orsi, A. Fluerasu, A. Moussaïd, F. Zontone, L. Cristofolini, and A. Madsen, Physical Review E **85**, 011402 (2012), publisher: American Physical Society.

- [8] M. Heinen, A. J. Banchio, and G. Nägele, *The Journal of Chemical Physics* **135**, 154504 (2011).
- [9] F. Westermeier, B. Fischer, W. Roseker, G. Grübel, G. Nägele, and M. Heinen, *The Journal of Chemical Physics* **137**, 114504 (2012).
- [10] F. Dallari, A. Jain, M. Sikorski, J. Möller, R. Bean, U. Boesenberg, L. Frenzel, C. Goy, J. Hallmann, Y. Kim, I. Lokteva, V. Markmann, G. Mills, A. Rodriguez-Fernandez, W. Roseker, M. Scholz, R. Shayduk, P. Vagovic, M. Walther, F. Westermeier, A. Madsen, A. P. Mancuso, G. Grübel, and F. Lehmkuhler, *IUCrJ* **8**, 775 (2021), publisher: International Union of Crystallography.
- [11] C. P. N. Tanner, V. R. K. Wall, J. Portner, A. Jeong, A. Das, J. K. Utterback, L. M. Hamerlynck, J. G. Raybin, M. J. Hurley, N. Leonard, R. B. Wai, J. A. Tan, M. Gababa, C. Zhu, E. Schaible, C. J. Tassone, D. T. Limmer, S. W. Teitelbaum, D. V. Talapin, and N. S. Ginsberg, *Enhancing nanocrystal superlattice self-assembly near a metastable liquid binodal* (2024), arXiv:2404.16808 [cond-mat].
- [12] P. N. Pusey and W. van Megen, *Journal de Physique* **44**, 285 (1983), publisher: Société Française de Physique.
- [13] W. van Megen and P. N. Pusey, *Physical Review A* **43**, 5429 (1991), publisher: American Physical Society.
- [14] U. Gasser, E. R. Weeks, A. Schofield, P. N. Pusey, and D. A. Weitz, *Science* **292**, 258 (2001), publisher: American Association for the Advancement of Science.
- [15] F. L. Calderon, J. Bibette, and J. Biais, *Europhysics Letters* **23**, 653 (1993).
- [16] J. R. Savage and A. D. Dinsmore, *Physical Review Letters* **102**, 198302 (2009).
- [17] N. A. M. Verhaegh, J. S. van Duijneveldt, J. K. G. Dhont, and H. N. W. Lekkerkerker, *Physica A: Statistical Mechanics and its Applications* **230**, 409 (1996).
- [18] A. R. Sandy, Q. Zhang, and L. B. Lurio, *Annual Review of Materials Research* **48**, 167 (2018), publisher: Annual Reviews.
- [19] G. Grübel, G. B. Stephenson, C. Gutt, H. Sinn, and T. Tschentscher, *Nuclear Instruments and Methods in Physics Research Section B: Beam Interactions with Materials and Atoms* **262**, 357 (2007).
- [20] F. Lehmkuhler, F. Dallari, A. Jain, M. Sikorski, J. Möller, L. Frenzel, I. Lokteva, G. Mills, M. Walther, H. Sinn, F. Schulz, M. Dartsch, V. Markmann, R. Bean, Y. Kim, P. Vagovic, A. Madsen, A. P. Mancuso, and G. Grübel, *Proceedings of the National Academy of Sciences* **117**, 24110 (2020), publisher: Proceedings of the National Academy of Sciences.
- [21] M. Sutton, S. G. J. Mochrie, T. Greytak, S. E. Nagler, L. E. Berman, G. A. Held, and G. B. Stephenson, *Nature* **352**, 608 (1991), publisher: Nature Publishing Group.
- [22] A. Fluerasu, M. Sutton, and E. M. Dufresne, *Physical Review Letters* **94**, 055501 (2005), publisher: American Physical Society.
- [23] O. G. Shpyrko, *Journal of Synchrotron Radiation* **21**, 1057 (2014).
- [24] M. Sutton, *Comptes Rendus. Physique* **9**, 657 (2008).
- [25] G. Grübel, A. Madsen, and A. Robert, in *Soft Matter Characterization*, edited by R. Borsali and R. Pecora (Springer Netherlands, Dordrecht, 2008) pp. 953–995.
- [26] M. Reiser, A. Girelli, A. Ragulskaya, S. Das, S. Berkowicz, M. Bin, M. Ladd-Parada, M. Filianina, H.-F. Poggemann, N. Begam, M. S. Akhundzadeh, S. Timmermann, L. Randolph, Y. Chushkin, T. Seydel, U. Boesenberg, J. Hallmann, J. Möller, A. Rodriguez-Fernandez, R. Rosca, R. Schaffer, M. Scholz, R. Shayduk, A. Zozulya, A. Madsen, F. Schreiber, F. Zhang, F. Perakis, and C. Gutt, *Nature Communications* **13**, 5528 (2022).
- [27] F. Lehmkuhler, J. Valerio, D. Sheyfer, W. Roseker, M. A. Schroer, B. Fischer, K. Tono, M. Yabashi, T. Ishikawa, and G. Grübel, *IUCrJ* **5**, 801 (2018), publisher: International Union of Crystallography.
- [28] I. Coropceanu, E. M. Janke, J. Portner, D. Haubold, T. D. Nguyen, A. Das, C. P. N. Tanner, J. K. Utterback, S. W. Teitelbaum, M. H. Hudson, N. A. Sarma, A. M. Hinkle, C. J. Tassone, A. Eychmüller, D. T. Limmer, M. Olvera de la Cruz, N. S. Ginsberg, and D. V. Talapin, *Science* **375**, 1422 (2022).
- [29] A. Nogales and A. Fluerasu, *European Polymer Journal* **81**, 494 (2016).
- [30] R. L. Leheny, *Current Opinion in Colloid & Interface Science* **17**, 3 (2012).
- [31] J. Möller, M. Sprung, A. Madsen, and C. Gutt, *IUCrJ* **6**, 794 (2019), publisher: International Union of Crystallography.
- [32] A. Jeong, J. Portner, C. P. N. Tanner, J. C. Ondry, C. Zhou, Z. Mi, Y. A. Tazoui, V. R. K. Wall, N. S. Ginsberg, and D. V. Talapin, *Colloidal dispersions of sterically and electrostatically stabilized PbS quantum dots: the effect of stabilization mechanism on structure factors, second virial coefficients, and film-forming properties* (2024), arXiv:2404.18915.
- [33] A. Madsen, J. Hallmann, G. Ansaldi, T. Roth, W. Lu, C. Kim, U. Boesenberg, A. Zozulya, J. Möller, R. Shayduk, M. Scholz, A. Bartmann, A. Schmidt, I. Lobato, K. Sukharnikov, M. Reiser, K. Kazarian, and I. Petrov, *Journal of Synchrotron Radiation* **28**, 637 (2021), publisher: International Union of Crystallography.
- [34] T. Tschentscher, C. Bressler, J. Grünert, A. Madsen, A. P. Mancuso, M. Meyer, A. Scherz, H. Sinn, and U. Zastrau, *Applied Sciences* **7**, 592 (2017), number: 6 Publisher: Multidisciplinary Digital Publishing Institute.
- [35] W. Decking, S. Abeghyan, P. Abramian, A. Abramsky, A. Aguirre, *et al.*, *Nature Photonics* **14**, 391 (2020), publisher: Nature Publishing Group.
- [36] B. Henrich, J. Becker, R. Dinapoli, P. Goettlicher, H. Graafsma, H. Hirsemann, R. Klanner, H. Krueger, R. Mazzocco, A. Mozzanica, H. Perrey, G. Potdevin, B. Schmitt, X. Shi, A. K. Srivastava, U. Trunk, and C. Youngman, *Nuclear Instruments and Methods in Physics Research Section A: Accelerators, Spectrometers, Detectors and Associated Equipment 11th International Workshop on Radiation Imaging Detectors (IWORID)*, **633**, S11 (2011).
- [37] We ascribe the dynamics of the quenched state to the NCs in the liquid phase since the scattering from the liquid phase is ~ 1 order of magnitude larger than that of the colloidal phase at the q values over which the correlation analysis is performed.
- [38] A. Madsen, R. L. Leheny, H. Guo, M. Sprung, and O. Czakkel, *New Journal of Physics* **12**, 055001 (2010).
- [39] J.-P. Hansen and L. Verlet, *Physical Review* **184**, 151 (1969).
- [40] P. N. Pusey, *Journal of Physics A: Mathematical and General* **8**, 1433 (1975).

- [41] F. Roosen-Runge, M. Hennig, F. Zhang, R. M. J. Jacobs, M. Sztucki, H. Schober, T. Seydel, and F. Schreiber, *Proceedings of the National Academy of Sciences* **108**, 11815 (2011), publisher: Proceedings of the National Academy of Sciences.
- [42] K. F. Seefeldt and M. J. Solomon, *Physical Review E* **67**, 050402 (2003).
- [43] C. Beenakker and P. Mazur, *Physica A: Statistical Mechanics and its Applications* **120**, 388 (1983).
- [44] C. W. J. Beenakker and P. Mazur, *Physica A: Statistical Mechanics and its Applications* **126**, 349 (1984).
- [45] T. K. Haxton, L. O. Hedges, and S. Whitelam, *Soft Matter* **11**, 9307 (2015).
- [46] W. C. K. Poon, A. D. Pirie, and P. N. Pusey, *Faraday Discussions* **101**, 65 (1995), publisher: Royal Society of Chemistry.
- [47] N. M. Kovalchuk and V. M. Starov, *Advances in Colloid and Interface Science Interfaces, Wettability, Surface Forces and Applications: Special Issue in honour of the 65th Birthday of John Ralston*, **179-182**, 99 (2012).
- [48] M. A. Boles, M. Engel, and D. V. Talapin, *Chemical Reviews* **116**, 11220 (2016).
- [49] C. B. Murray, C. R. Kagan, and M. G. Bawendi, *Science* **270**, 1335 (1995).
- [50] E. V. Shevchenko, D. V. Talapin, N. A. Kotov, S. O'Brien, and C. B. Murray, *Nature* **439**, 55 (2006).
- [51] D. K. Smith, B. Goodfellow, D.-M. Smilgies, and B. A. Korgel, *Journal of the American Chemical Society* **131**, 3281 (2009).
- [52] K. Bian, J. J. Choi, A. Kaushik, P. Clancy, D.-M. Smilgies, and T. Hanrath, *ACS Nano* **5**, 2815 (2011).
- [53] P. J. Santos, P. A. Gabrys, L. Z. Zornberg, M. S. Lee, and R. J. Macfarlane, *Nature* **591**, 586 (2021).
- [54] P. G. Debenedetti, *Metastable Liquids: Concepts and Principles*, Vol. 1 (Princeton University Press, 1996).
- [55] C. N. Nanev, in *Handbook of Crystal Growth (Second Edition)*, edited by T. Nishinaga (Elsevier, Boston, 2015) pp. 315–358.
- [56] M. Uwaha, in *Handbook of Crystal Growth (Second Edition)*, edited by T. Nishinaga (Elsevier, Boston, 2015) pp. 359–399.
- [57] J. F. Brady and G. Bossis, *Annual Review of Fluid Mechanics* **20**, 111 (1988), publisher: Annual Reviews.
- [58] A. J. Banchio and J. F. Brady, *The Journal of Chemical Physics* **118**, 10323 (2003).
- [59] T. N. Phung, J. F. Brady, and G. Bossis, *Journal of Fluid Mechanics* **313**, 181 (1996).
- [60] M. G. Noro, N. Kern, and D. Frenkel, *Europhysics Letters* **48**, 332 (1999), publisher: IOP Publishing.
- [61] J. Israelachvili, *Intermolecular and Surface Forces*, 3rd ed. (Elsevier, Inc., 2011).
- [62] S. Asakura and F. Oosawa, *The Journal of Chemical Physics* **22**, 1255 (1954).
- [63] S. Asakura and F. Oosawa, *Journal of Polymer Science* **33**, 183 (1958).
- [64] A. Vrij, *Pure and Applied Chemistry* **48**, 471 (1976), publisher: De Gruyter.